54th AIAA Aerospace Sciences Meeting
4 - 8 Jan 2016, San Diego, CA
AIAA-2016-1586

Optical Characterization of Nozzle-Wall Mach-6 Boundary Layers

Stanislav Gordeyev[1] and Thomas J. Juliano[2],
Department of Aerospace and Mechanical Engineering,
University of Notre Dame, Notre Dame, IN 46556

This paper presents the results of experimental investigation of aero-optical distortions caused by turbulent and laminar boundary layers in the Boeing/AFOSR Mach-6 Quiet Tunnel at Purdue University. Using optical window inserts installed in the test section, aero-optical distortions of the turbulent boundary layer at different freestream pressures were measured with a high-speed wavefront sensor at sampling speeds up to 1 MHz. Temporal and spatial statistics of the related aero-optical structure were measured and found to be quite similar to the ones at subsonic and low supersonic speeds. The existing model was found to under-predict the experimentally-measured levels of aero-optical distortions for turbulent boundary layers by 20%; possible reasons for this discrepancy are discussed. Intermittent turbulent spots and single-mode transitional events in the laminar boundary layers were observed and briefly analyzed.

Nomenclature

Ap	=	aperture size
AF	=	aperture filter, defined in [3]
Cf	=	skin friction
f	=	frequency
F	=	Mach-dependent function, Eq. (3)
G	=	aperture function, defined in Eq. (1a)
K_{GD}	=	Gladstone-Dale constant
M	=	Mach number
n	=	index of refraction
OPD	=	optical path difference
OPD_{rms}	=	spatial r.m.s. of OPD
St_δ	=	Strouhal number (= $f\delta/U_\infty$)
P0	=	plenum pressure
t	=	time
T0	=	plenum temperature
U_C	=	convective speed
x,y,z	=	spatial coordinates
W	=	wavefront
$W1$	=	one-dimensional wavefront
δ	=	boundary layer thickness
ρ	=	density
ρ_x^{1-D}	=	streamwise correlation function
ρ_z^{1-D}	=	spanwise correlation function
θ	=	deflection angle amplitude spectrum

Subscripts

∞	=	freestream value

I.Introduction

AERO-OPTICAL effects [1,2] are the result of the dependence of the index-of-refraction, n, on the density in air, ρ, via the Gladstone-Dale constant, K_{GD} (which is approximately 2.27×10^{-4} m^3/kg in air for visible wavelengths of light), $n(\vec{x},t)-1=K_{GD}\rho(\vec{x},t)$. Light passing through regions of unsteady turbulent flow is distorted by the spatially- and temporally-fluctuating density fields present along the optical path length. The effect of turbulent density fluctuations on the propagation of light can be quantified by defining the Optical Path Difference (OPD) as the

[1] Research Associate Professor, Department of Mechanical and Aerospace Engineering, Hessert Laboratory for Aerospace Research, Notre Dame, IN 46556, AIAA Associate Fellow.
[2] Assistant Professor, Department of Mechanical and Aerospace Engineering, Hessert Laboratory for Aerospace Research, Notre Dame, IN 46556, AIAA Senior Member.

average-removed integral of the index-of-refraction of a medium along the physical length traversed by a ray of light,

$$OPD(x,y,t) = \int n'(x,y,z,t)dz = K_{GD} \int \rho'(x,y,z,t)dz$$

where primes denote mean-removed fluctuations and z is the direction of beam propagation.

While the aero-optics of subsonic boundary layers has been extensively studied in recent years [2,3 and references therein], experimental measurements [4,5,6] and numerical simulations [7,8,9] in high supersonic and hypersonic boundary layers are very limited and many important questions about the details of the underlying aero-optical structure and its dynamics still remain unanswered. Several theoretical models were proposed [4,5] to predict levels of aero-optical distortions caused by supersonic boundary layers at different Mach and Reynolds numbers, but additional experimental data are still needed to fully verify them at high speeds. Also, the non-intrusive nature of aero-optical measurements makes them very attractive to study transitional hypersonic boundary layers, which generally are very sensitive to any surface-mounted sensors.

The state of a hypersonic boundary layer --- whether it is laminar, transitional, or turbulent --- is an important factor in the design of hypersonic vehicles due to its effect on surface heating, skin friction, separation, aero-optical distortion, and other boundary-layer properties [10]. Thus, the boundary-layer state's aero-optical impact can be exploited as a means to study the boundary layer. In this experiment, a Shack-Hartmann wavefront sensor, which non-intrusively measures density fluctuations, was used to investigate a hypersonic boundary layer. This technique offers several advantages. For example, the interrogation region can be smaller than that of a typical pressure transducer. Additionally, the boundary-layer density fluctuation spectrum can be assessed simultaneously with the wall shear stress. One wavefront sensor can replace several individual transducers for the measurement of convective speeds and directions of density fluctuations, thus *a priori* knowledge of the disturbances to optimize sensor installation is not required.

II.Experimental Set-Up

The data presented herein were collected in the Boeing/AFOSR Mach-6 Quiet Tunnel (BAM6QT) at Purdue University. The Ludwieg tube configuration is shown in Figure 1. The BAM6QT employs many features to maintain a laminar nozzle-wall boundary layer, thereby achieving quiet flow. The valve in the bleed-slot suction plumbing can be set to open or remain closed during a run, permitting the user to control whether the nozzle-wall boundary layer is laminar (for quiet flow) or turbulent (noisy flow). While running quietly, the noise level is less than 0.05%, and it increases to about 3% when noisy [11]. A more comprehensive discussion of the components of the BAM6QT is contained in [12].

The air is heated to a nominal stagnation temperature of 433 K, corresponding to a static temperature of 53 K when expanded to Mach 6. The freestream Mach number in the test section is 6.0 under quiet flow and varies slightly with stagnation pressure. Thicker, turbulent nozzle-wall boundary layers reduce the freestream Mach number to 5.8 when running with conventional noise levels.

The BAM6QT test section accommodates several interchangeable inserts [13]. For these tests, two windows with 40-mm viewable diameters were installed at an axial station 1.924 m from the nozzle throat in the forward ports of the "small" 3x10-in. inserts [14].

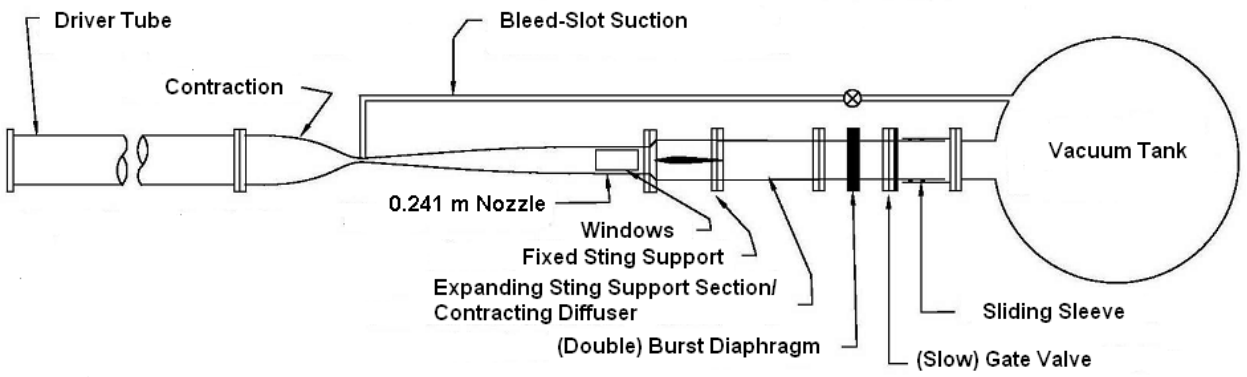

Figure 1: BAM6QT schematic.

Several runs with different stagnations pressures and with either turbulent or laminar boundary layers were performed, see Table 1. In order to establish boundary-layer parameters at different tunnel regimes, numerical simulations were performed for different stagnation pressures between 50 and 150 psia by Dr. Bradley Wheaton using the Sivells method of characteristics code [15] and the Harris finite-difference boundary-layer code [16]. Wheaton's laminar boundary-layer simulations are reported in Ref. [17] and showed good agreement with experimentally measured laminar boundary layers; the simulations of turbulent boundary layers were newly generated for this report. The computed boundary layer thicknesses and skin frictions are presented in Table 1. For the turbulent boundary layers, Re_θ was found to be approximately between 4,600 for P_0 = 90 psia and 6,860 for P_0 = 145 psia.

Table 1. Initial flow parameters and computed boundary-layer properties.

Run	P_0, psia	T_0, C	ρ_∞, kg/m^3	δ, mm	C_f	BL	Aperture location
Run A2	143	159	0.0413	29.6	$9.1\text{x}10^{-4}$	turbulent	centerline
Run A3	138	156	0.0401	6.1	$3.2\ \text{x}10^{-5}$	laminar	centerline
Run A4	91	160	0.0262	31.6	$9.9\text{x}10^{-4}$	turbulent	centerline
Run A5	93	157	0.0270	7.7	$4.0\ \text{x}10^{-5}$	laminar	centerline
Run A6	145	156	0.0422	29.5	$9.1\text{x}10^{-4}$	turbulent	7 mm above centerline
Run A7	145	152	0.0426	6.1	$4.0\ \text{x}10^{-5}$	laminar	7 mm above centerline
Run B1	143	157	0.0413	29.6	$9.1\text{x}10^{-4}$	turbulent	Full 2-D aperture
Run B8	175	151	0.0504	5.6 (estimate)	$9.1\text{x}10^{-4}$ (estimate)	laminar	10 mm above centerline

All measurements of wavefronts were performed using a high-speed Shack-Hartmann WaveFront Sensor, WFS; a schematic of the experimental set-up for Runs A2-A7 are shown in Figure 2. The laser beam was expanded to 50-mm-diameter and passed perpendicularly through two window inserts mounted in the test section. The first window had two flat parallel surfaces, labelled "Flat Insert" in Figure 2. The centerline of the first insert was flush with the tunnel wall, with an increasing step away from the centerline. The second insert had one flat and one contoured surface, matching the curvature of the test section (called "Contoured Insert" in Figure 2). When passed through the test section, the laser beam encountered two hypersonic boundary layers, one on each side of the test section. After a series of contracting and compensating optical elements,

the laser beam was reduced to a 10-mm diameter and was sent to a high-speed digital camera, Phantom v1610. The camera had a 38-mm-focal-length, 70x60-lenslet, 0.3-mm-pitch array attached to it. After passing through the lenslet array, the beam was split into subaperture beams and focused on the camera sensor, creating a series of dots. To achieve the high sampling rate of 1,000,000 fps, only a small, 16x218-pixel portion of the image was sampled for 4 seconds (Figure 4).

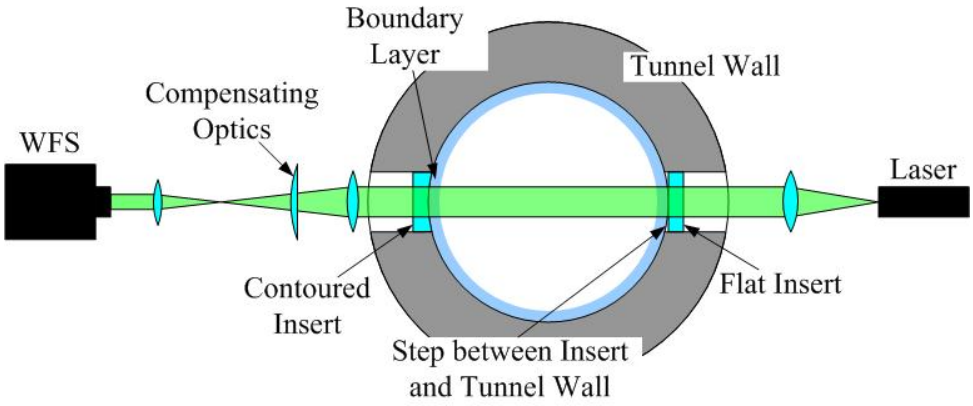

Figure 2. Schematics of single-path BL experimental set-up.

Runs A2-A5 were performed with the measured portion of the beam along the centerline of both inserts, so there was nominally no step between the flat insert and the contoured tunnel wall at this measurement location. For the last two runs, Run A6 and Run A7, the beam was shifted 7 mm up, so a small step of approximately 0.2 mm was present upstream of the measurement location, tripping the boundary layer over the flat insert.

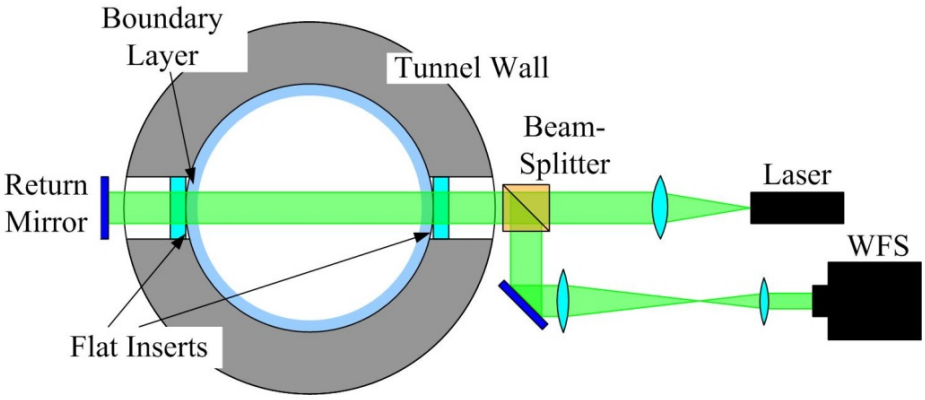

Figure 3. Schematics of double-path BL experimental set-up.

As the inner surface of the contoured insert was not exactly cylindrical, it introduced additional optical distortions on the resulting beam. To eliminate them, additional wavefront measurements, Run B1 and Run B8 in Table 1, were performed with two flat inserts installed on both sides on the tunnel. The set-up for these measurements is shown in Figure 3 and was similar to the one shown in Figure 2, except that the 50-mm beam, after passing through the test section, was reflected back along the same path using the return mirror. In this case the beam traveled through the flow of interest twice. This so-called double-pass experiment increases the signal by the factor of two and allows placing all optical components on one side of the tunnel. The returning

beam was split off using a cube beam splitter, contracted to a 15-mm diameter using a contracting telescope and finally sent to the wavefront sensor. During Run B2 full 2-D wavefronts with 41x41 subaperture resolution were captured with the sampling frequency of 49 kHz for 1.2 seconds. For comparison purposes, the same small, 16x128-pixel, portion of the image, shifted up by 10 mm, was sampled for 4 seconds during Run B8.

III.Data Collection and Reduction

As stated before, a small portion of the dot pattern consisting of a streamwise line of 11 dots, seen in Figure 4, was sampled at a sampling rate of 1,000,000 frames-per-second. Temporal evolutions of the dots' centroids were extracted using in-house software and converted into time-series deflection angles at different spatial locations. These measurements are essentially equivalent to measurements using a multi-beam Malley probe [3,6]. An example of time-series of the deflection angle at one location is presented in Figure 5. The flow started, when the diaphragms ruptured, resulting in the tunnel shaking in the streamwise direction. The initial shaking is evident between during first 0.2 seconds of the run, with attenuating oscillations during the first 2 seconds. To minimize the corrupting effects of the tunnel shaking, 1-second-duration data (total of 1,000,000 points) 2 seconds after the start of the tunnel were used in the analysis.

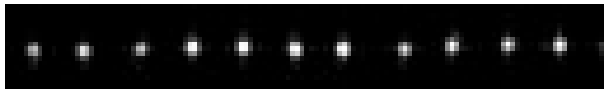

Figure 4. 11 x 1 wavefront image.

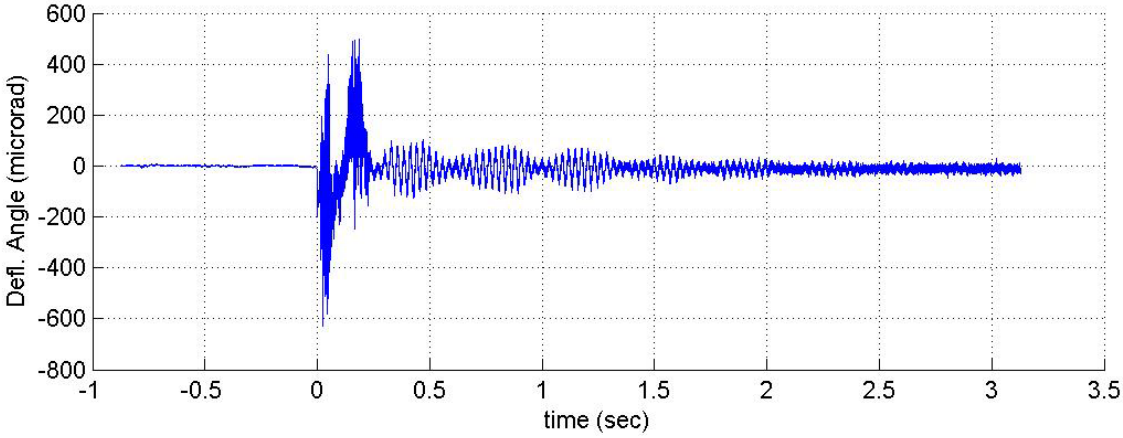

Figure 5. Time series of the one deflection angle during the run.

Deflection angles at multiple spatial points were Fourier-transformed to calculate deflection-angle spectra. Also, by performing a spectral cross-correlation at different spatial points, the convective speed of aero-optical structures can be calculated. The slope of the argument of the spectral cross-correlation function is proportional to convective time delay and, knowing the spatial separation between the beams, the convective speed of aero-optical structures can be calculated [3]. An example of the argument of the cross-correlation function for Run A2 is shown in Figure 6, top, with the corresponding convective speed of 831 m/sec.

If the convective speed is known, the total spectrum can be split into traveling, $\theta_T(f)$, and stationary, $\theta_S(f)$, spectra, using a multi-point cross-correlation technique, outlined in [6]. An example of the total, travelling and stationary components of the spectrum is shown in Figure 6, bottom. The stationary spectrum corresponds to mechanically-induced jitter due to the tunnel motion at low frequencies below 1 kHz. Above 1 kHz, the total and traveling spectra are virtually

identical, except at the very high end of the spectrum, where the total spectrum shows some evidence of spectral aliasing.

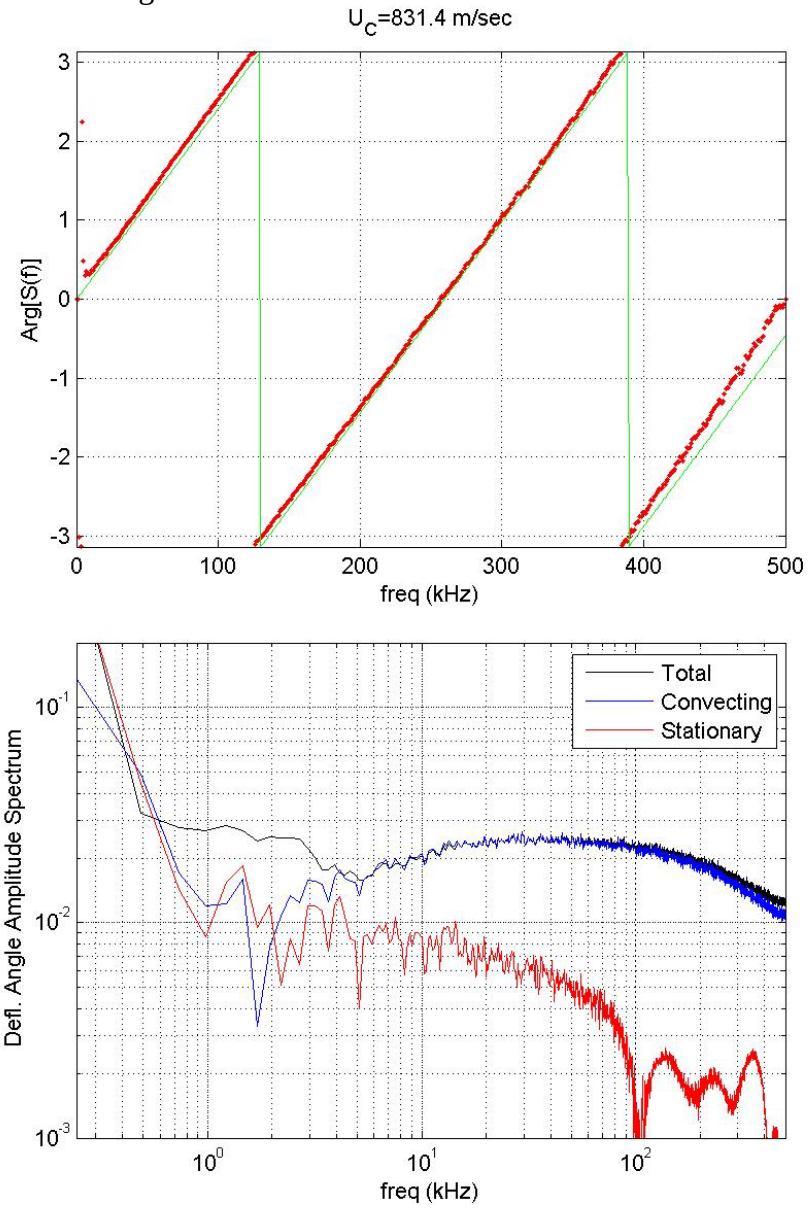

Figure 6. Top: Argument of the spectral cross-correlation function (red dots) for Run A2 with a linear fit (green line). Bottom: Total, traveling and stationary components of the deflection-angle amplitude spectrum for Run A2.

Finally, using the frozen field assumption, various important characteristics of the BL-related aero-optical distortions, such as an overall level of aero-optical distortions, OPD_{rms} and the aperture function, $G(Ap)$, were calculated from the traveling portion of the deflection-angle spectrum [3],

$$OPD_{rms}^2 = 2U_c \int_0^\infty \frac{\left|\hat{\theta}_T(f)\right|^2}{(2\pi f)^2} df \tag{1a}$$

$$G(Ap/\delta) \equiv OPD_{rms}(Ap)/OPD_{rms}, \quad where$$
$$OPD^2_{rms}(Ap) = 2U_c \int_0^\infty AF(Ap, f) \frac{\left|\hat{\theta}_T(f)\right|^2}{(2\pi f)^2} df \tag{1b}$$

Two-dimensional wavefronts from Run B1 were reduced using in-house software. The instantaneous piston and tip/tilt was removed from each wavefront. Spatial variation of wavefronts, $OPD_{\rm rms}(t;Ap)$, was calculated as, $OPD_{rms}(t;Ap) = \sqrt{\left\langle W(\vec{x},t)^2 \right\rangle_{\vec{x}\in Ap}}$ and time-averaged level of aero-optical distortions, $OPD_{\rm rms}(Ap)$ was computed by time averaging $OPD_{\rm rms}(t;Ap)$. Note that this value is just another way of computing $OPD_{\rm rms}(t;Ap)$, defined in Eq. (1b), but only for one aperture size.

In addition, one-dimensional "slices" of 2-D wavefronts in streamwise and spanwise directions were extracted, $W1(x,t) = W(x,z = 0,t)$ and $W1(z,t) = W(x=0,z,t)$. After removing instantaneous one-dimensional piston and tilt from each wavefront, one-dimensional correlation functions in the streamwise direction, $\rho_x^{1-D}(\Delta x; Ap) = \frac{1}{Ap} \int_{-Ap/2+\Delta x}^{Ap/2} \overline{W1(x,t)W1(x-\Delta x,t)} dx$, and the spanwise direction, $\rho_z^{1-D}(\Delta z; Ap) = \frac{1}{Ap} \int_{-Ap/2+\Delta x}^{Ap/2} \overline{W1(z,t)W1(z-\Delta z,t)} dz$, were calculated. Both these functions are also functions of the aperture size; for detailed discussion of aperture effects on aero-optical measurements in boundary layers the reader is referred to [3].

IV.Results

Turbulent boundary layers

Total deflection angle amplitude spectra for different cases, normalized by ρ_∞, are shown in Figure 7. The spectra for turbulent boundary layers for the plenum pressures of 143 psia (Run A2) and 91 psia (Run A4) collapse onto each other, confirming that the aero-optical distortions, for a fixed Mach number, are proportional to $\rho_\infty \delta$. The peak of the spectra is around 40 kHz. The spectrum of the turbulent boundary layer with the small upstream step (Run A6) is almost identical to the no-step case (Run A2); this result is expected, as the step size was only 0.6% of the turbulent boundary layer thickness.

The spectrum of the no-step laminar layer for P0 = 138 psia (Run A3), presented in Figure 7, and the analysis of the argument of the spectral cross-correlation function (not shown) did not reveal any traveling structures. However, when the plenum pressure was increased to 175 psia (Run B8), an increased spectrum, compared to the laminar spectrum, is evident in Figure 7. Analysis of this run had shown the presence of both the short-lived turbulent spots and second-mode transitional instability structures; some results will be briefly discussed in the end of this paper and detailed analysis will be given in [25]. Overall, Figure 7 demonstrates that this non-intrusive optical technique can clearly distinguish between different states of the boundary layers, suggesting a potential use as boundary-layer diagnostic tool at hypersonic speeds.

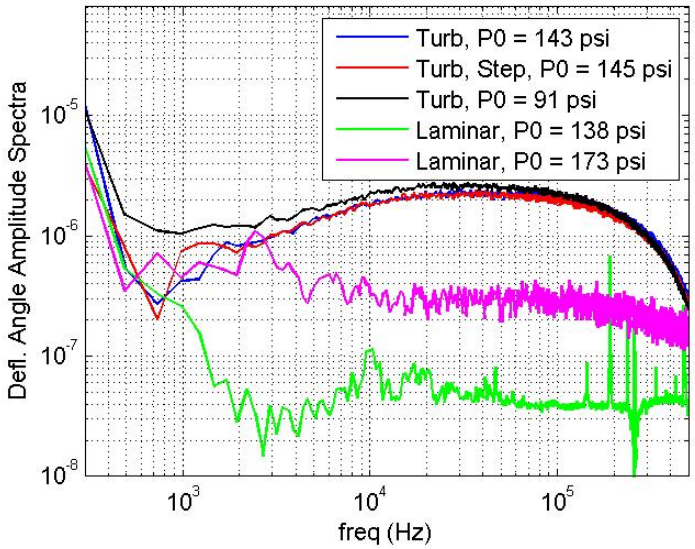

Figure 7. Deflection-angle spectra for various plenum pressures and BL states.

A normalized deflection-angle spectrum for the turbulent boundary layer is compared to the deflection-angle spectra at other supersonic Mach numbers from [18] in Figure 8. All spectra approximately collapse into each other, with small deviations at high St_δ, indicating that the large-scale structure, which is responsible for most of the aero-optical distortions, does not change significantly with the Mach number. The peak in all spectra is at approximately at $St_\delta = 1$, implying that the large-scale structure is on the order of the boundary layer thickness. The fact that the spectral peak location is the same of a wide range of Mach numbers, including the subsonic regime [3], is a very useful result, as it provides non-intrusive means to measure the turbulent boundary layer thickness over a wide range of Mach numbers by simply sending a small-aperture laser beam normal to the boundary layer and finding the location of the deflection angle peak.

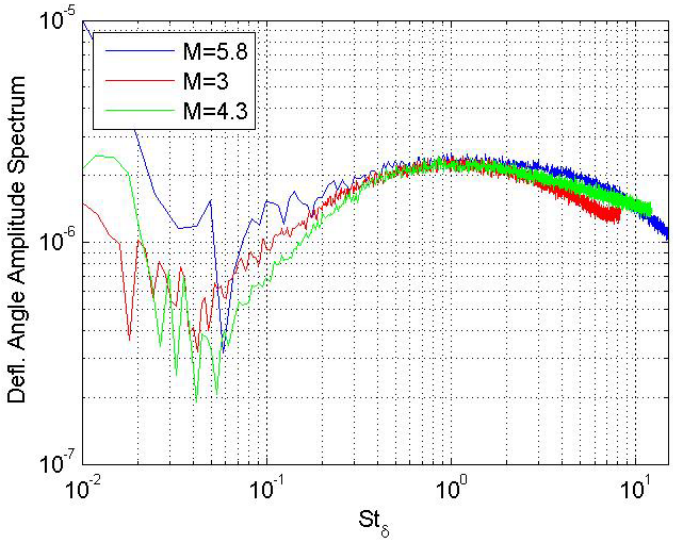

Figure 8. Normalized deflection angle spectrum for the turbulent boundary layer as a function of normalized frequency, $St_\delta = f\delta/U_\infty$, compared to the turbulent boundary-layer spectra at different supersonic Mach numbers from [18].

By cross-correlating deflection angles in the spectral domain, the convective speeds of aero-optical distortions were extracted and the results are presented in Figure 9, along with experimental results from [3,4,18]. Convective speeds are observed to monotonically increase with the Mach number, from $0.82U_\infty$ at subsonic speeds to $0.95U_\infty$ at M = 5.8. This effect of increasing the convective speed with Mach numbers was addressed in [4,18], where a model for boundary-layer aero-optical distortions was developed. The model showed that density fluctuations for supersonic speeds were suppressed near the wall due to higher flow temperatures near the wall and, therefore, aero-optical structures near the wall were less "optically" visible. Thus, aero-optical structures away from the wall were relatively stronger, resulting in higher observed aero-optical convective speeds at supersonic speeds. In [19] numerical simulations of aero-optical distortions for Mach numbers of 0.9 and 2.3 were performed and it was also observed that, while for the M = 0.9 case density fluctuations were approximately constant throughout the boundary layer, for the M = 2.3 case, density fluctuations in the outer part of the boundary layers were stronger than the ones near the wall. Similar trends of the wall-normal distribution of the density fluctuations were observed in [20], where supersonic boundary layers at M = 3, 4.5 and 6 were numerically simulated.

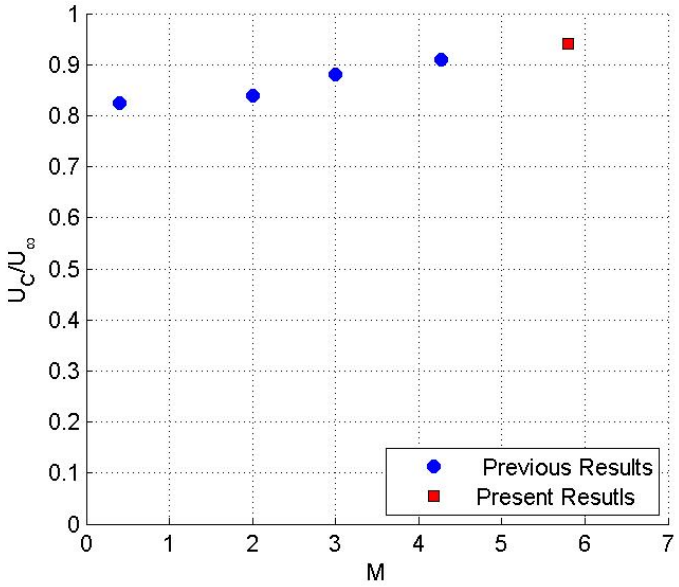

Figure 9. Experimentally-measured normalized convective speeds of aero-optical structures from the present study and from [3,4,18].

Using the deflection-angle spectrum, the aperture function $G(Ap/\delta) \equiv OPD_{rms}(Ap)/OPD_{rms}$ in Eq (1a) was computed and the result is plotted in Figure 10. The aperture function describes how aero-optical distortions are reduced for small apertures (order of the boundary layer thickness or less). The reason for this decrease is that instantaneous piston and tip/tilt are removed from the wavefronts; this removal procedure works as a high-pass filter, reducing the observed optical effect of the large-scale structure for small-aperture beams [22,23]. Direct optical measurements of apertured 2-D wavefronts (RunB1), presented in Figure 10, agree well with the aperture function, computed from deflection angle spectra. Comparison with the aperture functions for lower supersonic [18] and subsonic [3] boundary layers shows that the aperture function does not significantly change with the Mach number, at least in the measured

range. This is expected result, as the deflection-angle spectra for different supersonic Mach numbers in Figure 8, used to compute the aperture functions, are very similar.

One-dimensional streamwise and spanwise correlation functions are presented in Figure 11. They are compared with experimental results for the subsonic boundary layer for the same aperture size [3], as well the empirical fit, presented in [3]. While both correlation function are similar to the subsonic ones, the minimum location of the streamwise correlation function in Figure 11, left, is shifted toward smaller $\Delta x/\delta = 0.35$, compared to $\Delta x/\delta = 0.4$ for the subsonic boundary layer. It suggests that the streamwise "size" of the aero-optical structure at high Mach numbers might be smaller than for the subsonic speeds, but additional studies are needed measure the cross-correlation function at different aperture sizes and different Reynolds numbers.

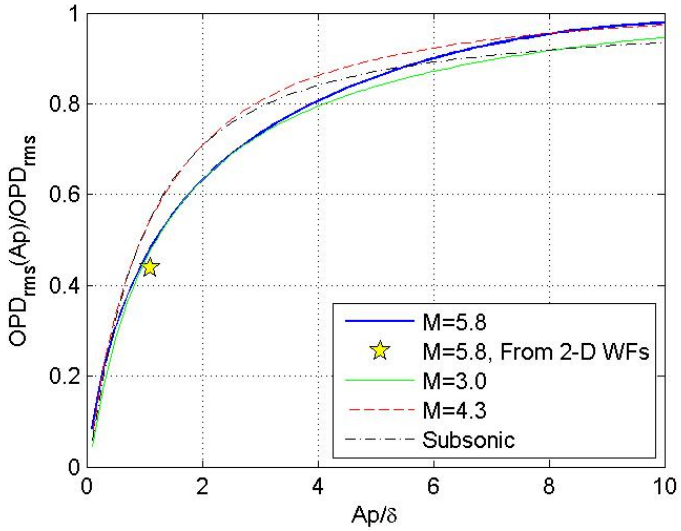

Figure 10. The aperture function, defined in Eq. (1a), computed from deflection angle spectra and from 2-dimensional wavefront data (Run B1) for M = 5.8. Results for M = 3.0 and 4.3 from [18] and for subsonic BL from [3] are also plotted for comparison.

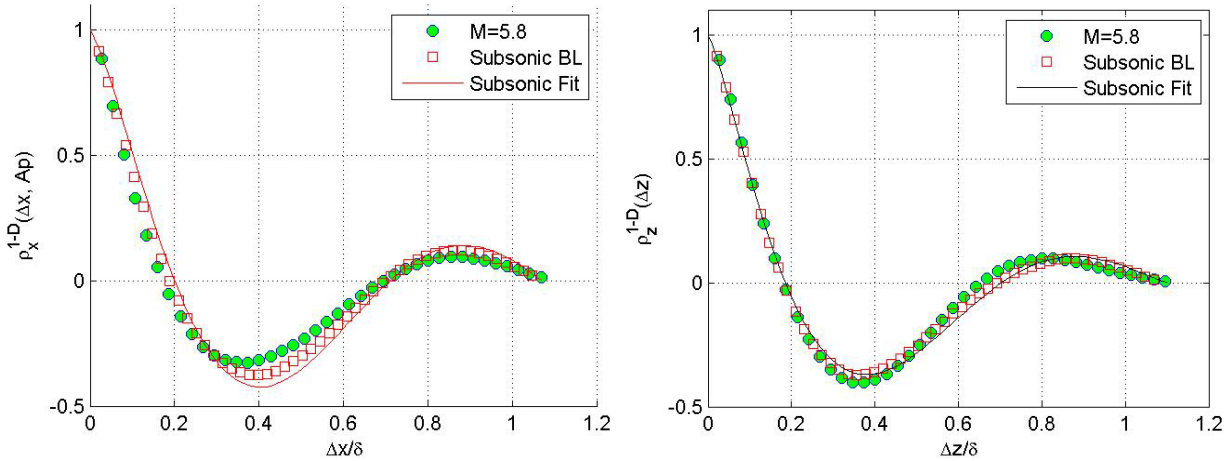

Figure 11. Streamwise (left) and spanwise (right) wavefront correlation functions using experimental 1-D wavefront slices from Run B1. Comparison with subsonic boundary results and the proposed empirical fit from [3] are also plotted for comparison.

In [3,21] the following model for boundary-layer aero-optical distortions was derived,

$$OPD_{rms} = 0.2K_{GD}\rho_\infty M_\infty^2 \delta\sqrt{C_f}F(M_\infty), \quad (3)$$

where C_f is the compressible skin friction and $F(M_\infty)$ was numerically estimated from velocity measurements; the F-function is shown in Figure 12 as a solid line. Results of recent studies of aero-optical aberrations at lower supersonic speeds [18] are also shown in Figure 12, showing the applicability of Eq. (3) up to M = 4.5. A model extension to non-adiabatic walls is presented in [21].

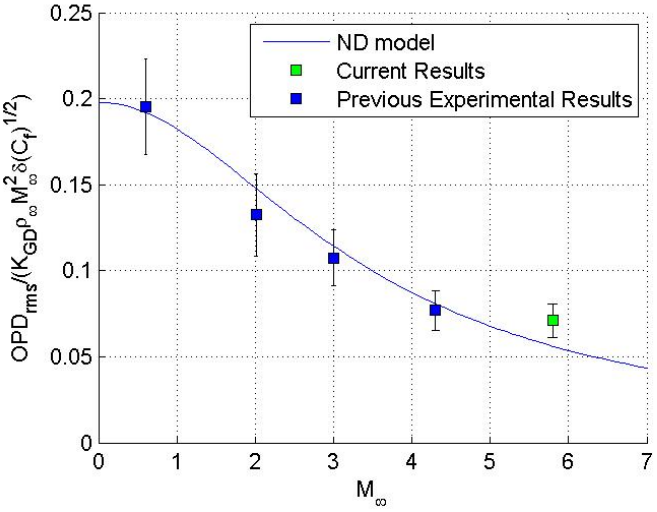

Figure 12. Normalized levels of OPD_{rms} at different Mach numbers and a model prediction from [18].

Knowing the convective speeds and the deflection-angle spectra, OPD_{rms} were calculated from 1-D wavefronts using Eq. (1a). OPD_{rms} values for the turbulent boundary layers for Runs A2, A4 and A6 were averaged and the results, normalized by $K_{GD}\rho_\infty M_\infty^2 \delta\sqrt{C_f}$, are plotted in Figure 12. The level of aero-optical distortions at M = 5.8 was found to be 20% higher than the model prediction, indicating that the model starts to be invalid for higher Mach numbers. It is an expected result, as many of the assumptions used to develop the model begin breaking up around M=3-5. The main assumptions used in developing the model are:

(a) all density fluctuations are due to adiabatic cooling/heating mechanism (Strong Reynolds Assumption).
(b) wall-normal density correlation function does not depend on the Mach number.

The first assumption ignores the pressure fluctuations inside the boundary layer. While it was shown to be a reasonable assumption at subsonic and low supersonic speeds, the analysis of the effect of the pressure, presented in [21], suggests that the relative importance of the pressure term increases with the local skin friction. As the skin friction goes up with the Mach number, it might be possible that the pressure term cannot be ignored in calculating aero-optical effects of turbulent boundary layer at transonic speeds.

The second assumption essentially states that the size of the large-scale structure in the wall-normal direction is not affected by the Mach number. As the density field develops a large density gradient near the wall at high Mach numbers, it will undoubtedly affect the development

of the large-scale structure. So, this assumption most certainly will not be valid at high speeds either and a more studies are needed to address this issue.

Nevertheless, the model still can be used to at least estimate the aero-optical distortions of turbulent boundary layers in the range of Mach numbers up to 6, which could be useful in designing various airborne laser-based systems.

Intermittent events in laminar boundary layer

While not the main topic of the paper, deflection angle signals for the laminar boundary layers were briefly examined. The signal at low plenum pressure of 138 psia, Run A4, exhibits only low-frequency, tunnel-vibration-related oscillations, indicating that the boundary layer was laminar during the run (not shown). However, when the plenum pressure increased to 175 psia during Run B8, the time series exhibit intermittent, short-time increases in the deflection angle amplitude, shown in Figure 13, top. Close inspection of the time series during one of these events reveals broad-spectrum fluctuations indicative of a turbulent boundary layer, see Figure 13, bottom. This flow feature, called turbulent boundary layer burst or spot, is well-known and was observed and documented in this tunnel by other researches [12,24]. From the aero-optical measurements, the typical spot duration was found to be 1.5 ms or ~ 180 δ/U_∞.

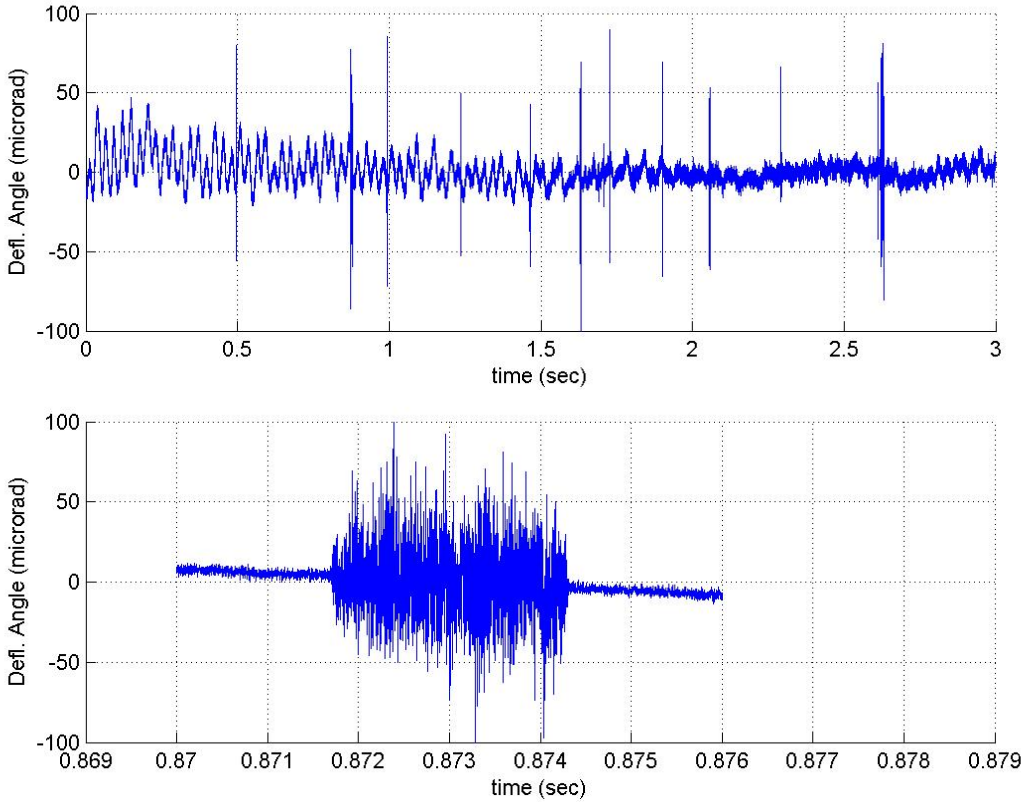

Figure 13. Time series of the deflection angle for high plenum pressure (top) and expanded view of the signal during "burst" turbulent event (bottom).

Time series inside these turbulent bursts were used to calculate the deflection angle spectra, which is presented in Figure 14 (red line). Comparison with the fully-turbulent spectrum from Run A2 (black line in Figure 14), indicated that the boundary layer is fully turbulent during these "bursts".

While inspecting deflection time series for Run B8, in addition to turbulent bursts, a different, single-frequency enveloped signal was observed, see Figure 15. This disturbance was only observed during the highest-pressure run: the initial stagnation pressure was 175 psia, close to the BAM6QT's maximum quiet pressure [24]. Spectra computed using several of these events are shown in Figure 16, along with the laminar boundary layer and the turbulent spot spectra for comparison. These single-mode events were found to correspond to a secondary transitional mode with the frequency of $0.5U_\infty/\delta$ ~80 kHz [17], indicated as a dashed line in Figure 16.

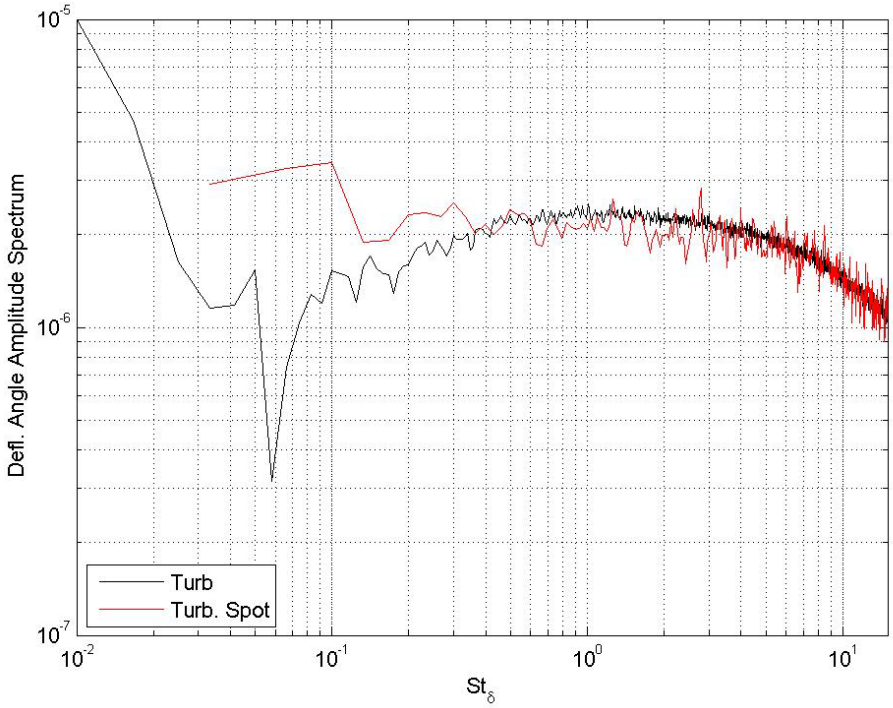

Figure 14. Comparison between the deflection angle spectra for the fully turbulent boundary layer and for the turbulent spot.

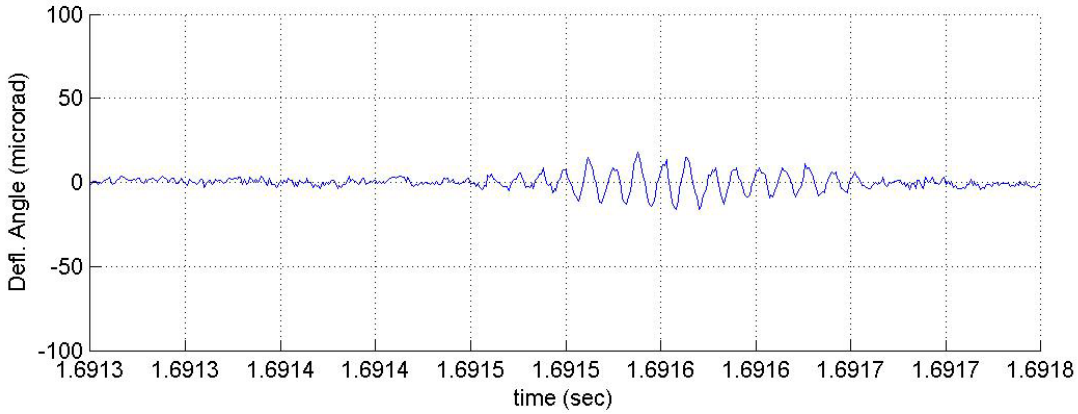

Figure 15. Portion of time series with a transitional single mode present.

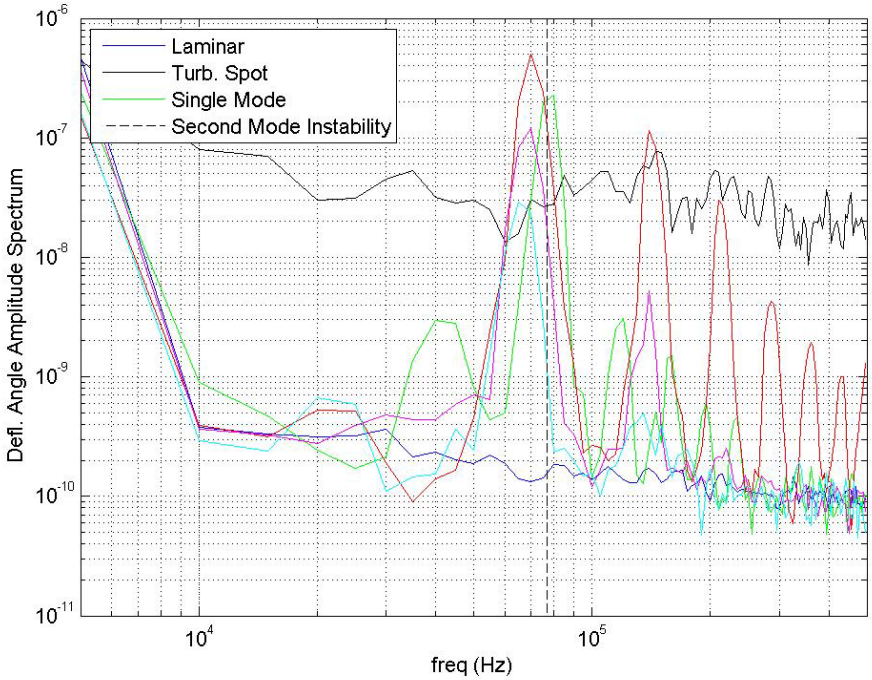

Figure 16. Deflection angle spectra of laminar BL (blue), during the turbulent spot (black) and during several single mode events (green, read and magenta). Theoretical prediction of the secondary instability mode from [17] is given as a vertical dashed line.

Analysis of the time series has shown that the duration of the single mode is between 0.1 and 0.2 ms or 12-25 δ/U_∞. So, these events are localized events, compared to the relatively large turbulent spots. Also, an average convective speeds of these structures was found to be U_C = 760 m/sec or U_C/U_∞ = 0.86. A detailed analysis and discussion of these localized turbulent and transitional events will be presented in a future paper [25].

V.Conclusions

Aero-optical effects from both turbulent and laminar boundary layers were investigated in in the Boeing/AFOSR Mach-6 Quiet Tunnel at Purdue University (BAM6QT), using a high-speed wavefront sensor. Deflection angles were collected at sampling speeds up to 1 MHz and the spectra and one-dimensional wavefronts were computed for different boundary layer states; limited two-dimensional wavefronts sequences were also collected. As expected, aero-optical spectra were found to scale with the freestream density and the presence of the small step around the optical inserts did not affect the levels of the spectra and related aero-optical distortions, at least over the optical windows. Assuming pure convective aero-optical distortions, an averaged convective speed of the aero-optical structure was computed as 0.95 of the freestream speed. Comparison with the convective speeds at lower Mach numbers revealed a monotonically-increasing trend of the convective speed with the Mach number. Comparison of the deflection-angle spectra and the one-dimensional spatial correlation functions with the ones at lower Mach numbers has concluded that the temporal and the spatial statistical properties of the underlying aero-optical structure does not significantly vary over a wide range of Mach numbers. Overall levels of aero-optical distortions of the turbulent boundary layers were computed at different freestream pressures. Comparison of

the levels with the existing model reveals that the model starts underestimating these levels by approximately 20% at this Mach number.

Although briefly, some results of the analysis of the aero-optical distortions of the laminar boundary layer are presented. They showed the evidence of the intermittent turbulent bursts or spots and, at the highest freestream pressure, the presence of intermittent single-mode transitional structures in the laminar boundary layer.

Overall, this paper has demonstrated the ability of the utilized optical technique of non-intrusively and accurately studying properties of both turbulent and laminar boundary layers at hypersonic speeds, for example the boundary layer thickness and the convective speed of aero-optical structures. It can be used, for instance, as non-intrusive diagnostic tool to quantify the state and parameters of the boundary layer.

Acknowledgements

The authors would like to thank Professor Steven Schneider of Purdue University for an opportunity to use BAM6QT to perform these measurements. We would like to express our gratitude to Dr. Bradley M. Wheaton of the Johns Hopkins University Applied Physics Laboratory for performing numerical simulations of the tunnel flow. We also thank Brandon Chynoweth of Purdue University and Dr. Amanda Chou of NASA Langley Research Center for their help preparing the experiment.

References

[1] Jumper, E.J. and Fitzgerald, E.J., 2001, "Recent Advances in Aero-Optics," *Progress in Aerospace Sciences*, 37, 299-339.

[2] Wang, M., Mani, A. and Gordeyev, S., "Physics and Computation of Aero-Optics", *Annual Review of Fluid Mechanics*, Vol. 44, pp. 299-321, 2012.

[3] Gordeyev, S., Smith, A.E., Cress, J.A. and Jumper, E.J. "Experimental studies of aero-optical properties of subsonic turbulent boundary layers," *Journal of Fluid Mechanics*, **740**, pp. 214-253, 2014.

[4] Gordeyev, S., Jumper, E.J. and Hayden, T., "Aero-Optics of Supersonic Boundary Layers," *AIAA Journal*, **50**(*3*), 682-690, 2012.

[5] Wyckham, C. and Smits, A. "Aero-Optic Distortion in Transonic and Hypersonic Turbulent Boundary Layers," *AIAA Journal*, **47**(*9*), pp. 2158-2168, 2009.

[6] A.E. Smith, S. Gordeyev, H. Ahmed, A. Ahmed, D.J. Wittich III and M. Paul, " Shack-Hartmann Wavefront Measurements of Supersonic Turbulent Boundary Layers in the TGF," AIAA Paper 2014-2493.

[7] E. Tromeur, E. Garnier and P. Sagaut, "Large-eddy simulation of aero-optical effects in a spatially developing turbulent boundary layer", *Journal of Turbulence*, Volume 7, 2006.

[8] E. Tromeur, P. Sagaut and E. Garnier, "Analysis of the Sutton Model for Aero-Optical Properties of Compressible Boundary Layers " *J. Fluids Eng.* **128**(*2*), 239-246, 2005.

[9] White, M. and Visbal, M., "Simulation of Aero-Optical Interactions in Transonic Boundary Layers," AIAA Paper 2011-3279, 2011.

[10] S.P. Schneider, "Laminar-Turbulent Transition on Reentry Capsules and Planetary Probes", *J. of Spacecraft and Rockets*, **43**(*6*) ,pp. 1153-1173, 2006.

[11] T. J. Juliano, S. P. Schneider, S. Aradag and D. Knight,"Quiet-Flow Ludwieg Tube for Hypersonic Transition Research", *AIAA Journal*, **46**(*7*), pp. 1757—1763, 2008.

[12] T.J. Juliano, "Nozzle Modifications for High-Reynolds-Number Quiet Flow in the Boeing/AFOSR Mach-6 Quiet Tunnel", PhD. Thesis, Purdue University, 2006.
[13] B. M. Wheaton and S. P. Schneider, "Roughness-Induced Instability in a Hypersonic Laminar Boundary Layer", *AIAA Journal*, **50**(*6*), pp. 1245—1256, 2012.
[14] A. Chou, "Mach-6 Receptivity Measurements of Laser-Generated Perturbations on a Flared Cone", PhD. Thesis, Purdue University, 2014.
[15] J. C. Sivells, "A Computer Program for the Aerodynamic Design of Axisymmetric and Planar Nozzles for Supersonic and Hypersonic Wind Tunnels", AEDC-TR-78-63, Arnold Engineering Development Center, Arnold Air Force Station, TN, December 1978.
[16] J. E. Harris and D. K. Blanchard, "Computer Program for Solving Laminar, Transitional, or Turbulent Compressible Boundary-Layer Equations for Two-Dimensional and Axisymmetric Flow", NASA TM 83207, NASA Langley Research Center, Hampton, VA, February, 1982.
[17] B. M. Wheaton, "Roughness-Induced Instabilities in a Mach-6 Laminar Boundary Layer", PhD. Thesis, Purdue University, 2012.
[18] S. Gordeyev, R.M. Rennie, A.B Cain and T. Hayden, “Aero-Optical Measurements of High-Mach Supersonic Boundary Layers”, AIAA Paper 2015-3246, 2015.
[19] E. Tromeur, E. Garnier, P. Sagaut and C. Basdevant, “Large eddy simulations of aero-optical effects in a turbulent boundary layer,” *Journal of Turbulence*, **4**, 005, 2003.
[20] T. Maeder, N.A. Adams and L Kleiser, “Direct simulation of turbulent supersonic boundary layers by an extended temporal approach,” *J. Fluid Mech*., **429**, pp. 187-216, 2001.
[21] S. Gordeyev, J.A. Cress, A. Smith and E.J. Jumper, “Aero-Optical Measurements in a Subsonic, Turbulent Boundary Layer with Non-Adiabatic Walls", *Physics of Fluids*, **27**, 045110, 2015.
[22] Siegenthaler, J., Gordeyev, S. & Jumper, E, “Shear layers and aperture effects for aerooptics,” AIAA Paper 2005-4772, 2005.
[23] Siegenthaler, J. P. Guidelines for adaptive-optic correction based on aperture filtration, PhD thesis, University of Notre Dame, 2008.
[24] K. M. Casper, “Hypersonic Wind-Tunnel Measurements of Boundary-Layer Pressure Fluctuations,” M.S. Thesis, Purdue University, 2009.
[24] B. C. Chynoweth, C. A. C. Ward, R. T. Greenwood, G. R. McKiernan, R. A. Fisher and S. P. Schneider, "Measuring Transition and Instabilities in a Mach 6 Hypersonic Quiet Wind Tunnel", AIAA Paper 2014-2643, 2014.
[25] S. Gordeyev and T.J. Juliano, “Optical Measurements of Transitional Events in a Mach-6 Laminar Boundary Layer,” an abstract submitted to AIAA Aviation and Aeronautics Forum and Exposition (AIAA AVIATION 2016), Washington, DC, 13 - 17 Jun 2016.